Artery Research (2016) 14, 41–52

Available online at www.sciencedirect.com

ScienceDirect

journal homepage: www.elsevier.com/locate/artres

Loss of elastic fiber integrity compromises common carotid artery function: Implications for vascular aging

J. Ferruzzi [a], M.R. Bersi [a], R.P. Mecham [b], F. Ramirez [c], H. Yanagisawa [d], G. Tellides [e,f], J.D. Humphrey [a,f,*]

[a] Department of Biomedical Engineering, Yale University, New Haven, CT, USA
[b] Department of Cell Biology, Washington University, St. Louis, MO, USA
[c] Departments of Pharmacology and Systems Therapeutics, Icahn School of Medicine at Mt. Sinai, New York, NY, USA
[d] Life Science Center, Tsukuba Advanced Research Alliance, University of Tsukuba, Ibaraki, Japan
[e] Department of Surgery, Yale School of Medicine, New Haven, CT, USA
[f] Vascular Biology and Therapeutics Program, Yale School of Medicine, New Haven, CT, USA

Received 25 November 2015; received in revised form 20 January 2016; accepted 1 April 2016
Available online 22 April 2016

KEYWORDS
Elastin;
Fibrillin-1;
Fibulin-5;
Elastic energy storage;
Distensibility;
Pulse wave velocity

Abstract Competent elastic fibers endow central arteries with the compliance and resilience that are fundamental to their primary mechanical function in vertebrates. That is, by enabling elastic energy to be stored in the arterial wall during systole and then to be used to work on the blood during diastole, elastic fibers decrease ventricular workload and augment blood flow in pulsatile systems. Indeed, because elastic fibers are formed during development and stretched during somatic growth, their continual tendency to recoil contributes to the undulation of the stiffer collagen fibers, which facilitates further the overall compliance of the wall under physiologic pressures while allowing the collagen to limit over-distension during acute increases in blood pressure. In this paper, we use consistent methods of measurement and quantification to compare the biaxial material stiffness, structural stiffness, and energy storage capacity of murine common carotid arteries having graded degrees of elastic fiber integrity – normal, elastin-deficient, fibrillin-1 deficient, fibulin-5 null, and elastase-treated. The finding that the intrinsic material stiffness tends to be maintained nearly constant suggests that intramural cells seek to maintain a favorable micromechanical environment in which to function. Nevertheless, a loss of elastic energy storage capability due to the loss of elastic fiber integrity severely compromises the primary function of these central arteries.

* Corresponding author. Department of Biomedical Engineering, Malone Engineering Center, Yale University, New Haven, CT 06520, USA. Tel.: +1 203 432 6428.
E-mail address: jay.humphrey@yale.edu (J.D. Humphrey).

http://dx.doi.org/10.1016/j.artres.2016.04.001

Introduction

The mechanical functionality, structural integrity, and adaptive capacity of central arteries result in large part from cellular regulation of the myriad structural constituents that constitute the wall, and their interactions. Notwithstanding the many contributors to the mechanics of the arterial wall, four are of primary importance: elastic fibers, fibrillar collagens, contractile smooth muscle, and proteoglycans/glycosaminoglycans.[1,2] Of these four, elastic fibers are unique - they alone do not turnover during maturity and they are not effectively repaired or replaced during disease or injury. That is, functional elastic fibers are produced prior to adulthood and they have a half-life on the order of 25–70 years in both mice and humans under normal conditions.[3–6] These fibers are thus uniquely susceptible to damage by mechanical fatigue in addition to normal degradation by proteolysis.[7–9] Because elastic fibers cannot be effectively repaired or replaced, congenital and acquired losses of elastic fiber integrity have irreversible consequences on arterial mechanics and mechanobiology, and thus the physiology and pathophysiology. Genetically induced changes in, proteolytic degradation of, or mechanical damage to elastic fibers contribute, therefore, to central artery stiffening in aging and hypertension, which in turn promote diverse cardiovascular, renovascular, and neurovascular diseases.[10–12] Indeed, loss of elastic fiber integrity also plays direct mechanical roles in atherosclerosis, aneurysms, and dissections.[13–15]

Elastic fibers in central arteries are organized into concentric fenestrated elastic sheets, or laminae, that form a three-dimensional network in the media. These fibers consist primarily of a core of elastin (90%) plus multiple elastin-associated glycoproteins.[2,16] The glycoproteins fibulin-5 and fibrillin-1 are fundamental to the elastogenesis and long term mechanical and biological stability, respectively, of the composite fibers.[17,18] Elastic fibers also associate with proteoglycans and minor collagens (e.g., collagen VIII), though specific contributions of these constituents to mechanical functionality is less clear.[16] Nevertheless, loss of elastic fiber integrity has five primary consequences to the arterial wall: loss of resilience and thus a decrease in elastic recoil,[19] decrease in collagen fiber undulation and thus diminished distensibility and extensibility,[20] loss of cell–matrix interactions and thus altered smooth muscle cell phenotypic activity,[17,21] increased intramural inflammation due to the chemotactic character of elastin degradation products,[9] and possible premature entrance into the cell death cycle, or anoikis.[22]

Among the many important consequences of reduced elastic fiber integrity, we focused on the mechanical functionality of the common carotid artery (CCA) in the mouse. Specifically, we contrasted passive biaxial mechanical behaviors of carotids from control, elastin haploinsufficient ($Eln^{+/-}$), fibrillin-1 deficient ($Fbn1^{mgR/mgR}$), and fibulin-5 null ($Fbln5^{-/-}$) mice with elastase-treated carotids from control mice. In this way, we assessed graded effects on wall structure and function due to elastic fibers ranging from normal to fully compromised. New biaxial data ($Eln^{+/-}$) are presented and compared with previously published data (controls from,[23] elastase-treated and $Fbn1^{mgR/mgR}$ from,[20] and $Fbln5^{-/-}$ from [24]) using new approaches for interpreting the data. By treating control and elastase-treated data as upper and lower bounds of elastic fiber functionality, respectively, we elucidated graded changes in carotid artery mechanics across the three genetic models. Importantly, total elastic energy displays a strong qualitative correlation with the severity of elastic fiber disarray.

Methods

Experimental methods

All animal protocols were approved by the Institutional Animal Care and Use Committee of Yale University. Briefly, mice were euthanized and CCAs were gently excised, cleaned of excess perivascular tissue, cannulated on custom drawn glass pipettes, and placed within a custom biaxial testing system in a Hanks buffered saline at 37 °C[25]; we have shown that this protocol yields a passive behavior.[20] Following methods described previously,[23] we performed cyclic pressure–diameter ($P–d$) tests at three different fixed axial stretches (the *in vivo* value and 5% above and below this value) and cyclic axial force–length ($f–l$) tests at four different fixed pressures (10, 60, 100, 140 mmHg). The latter tests are particularly important for estimating the preferred, or optimal, *in vivo* axial stretch[26] and ensuring robust estimations of material parameters that define biaxial wall properties.[23] All data (luminal pressure, outer diameter, axial force, and axial length, noting that axial stretch is defined as the ratio of the *in vivo* to the unloaded *in vitro* length) were collected using a custom LabView program and used for on-line feedback control of the tests and off-line analysis.

Material characterization

Each of the seven biaxial protocols (three $P–d$ plus four $f–l$) consisted of two cycles of data. We extracted and combined the unloading portion of the final cycle for the seven data sets, each of which consisted of hundreds of data points. The unloading portion of a testing cycle provides information on the energy stored in the tissue that is yet available to work on the blood; that is, it does not include the small amount (typically 3–5%) of energy that dissipates during full pressure–diameter and axial force–length testing. The resulting combined data sets were analyzed via nonlinear regression to identify best-fit values of model parameters in a validated constitutive relation. Details on the constitutive formulation and regression method are given elsewhere.[23,27] Briefly, we use a stored-energy function W containing 8 parameters $(c, c_1^1, c_2^1, c_1^2, c_2^2, c_1^{3,4}, c_2^{3,4}, \alpha_o)$ to model contributions to overall load bearing within the wall by an elastin-dominated isotropic matrix and four families of locally-parallel fibers; these fiber families are set in axial, circumferential, and symmetric diagonal directions to capture phenomenologically the net effects of distributed collagen fibers and their lateral cross-links as well as, in the circumferential direction, passive smooth muscle cells (see Appendix). This constitutive relation describes and predicts well the passive

biaxial mechanical responses of multiple elastic arteries from mice.[20,28–30] Importantly, because it is written directly in terms of elastic energy storage, per unit undeformed volume, it reflects intrinsic material properties. Values of biaxial stress and stiffness are computed easily via appropriate first and second derivatives of this single scalar energy function (see Appendix).

Physiological predictions

The primary loads acting on the CCA *in vivo* are an axial stretch-associated axial force and the transmural pressure. The former, which results primarily from somatic growth, is controlled locally by intramural cells and can change over time due to growth and remodeling.[26] Multiple studies confirm that the associated value of *in vivo* axial stretch can be inferred via a "cross-over point" in *in vitro* f–l tests.[31,32] The *in vivo* transmural pressure is influenced by systemic factors, notably cardiac output and peripheral vascular resistance, and by local effects of perivascular tissues. The latter are difficult to assess, hence transmural pressures are typically assumed to be slightly below measured luminal pressures. We extracted blood pressure data from the literature that were collected invasively under anesthesia, thus representing direct measurements of central blood pressure. Our selection criteria included the need to match mouse genotype and age with those animals that underwent biomechanical testing. Final values are listed in Table 1 and discussed below.

Mutations of genes that code elastic fiber proteins affect blood pressure,[33] but variations due to experimental conditions - including depth of anesthesia - are important as well. Thus, we performed a sensitivity analysis to understand how changes in pressure affect the biomechanical metrics of interest for the different groups studied. Specifically, we assessed different mechanical metrics of interest over transmural pressures from 50 to 150 mmHg, in increments of 10 mmHg, to cover a wide range of physiologic values.

Statistical analysis

All data are reported as mean ± the standard error of the mean (SEM). Comparisons between groups were made using a one-way ANOVA with post-hoc Bonferroni correction and a value of $p < 0.05$ considered significant. Significant difference from control is indicated in figures and tables, were appropriate.

Table 1 Mean physiologic and mechanical data for common carotid arteries. Systolic and pulse pressures were extracted from [a]Le et al.,[47] [b]Le et al.,[53] and [c]Marque et al.[40] We used data for C57BL/6J and *Eln*$^{+/-}$ mice, from[47] and on mixed C57BL/6J × 129/SvEv, as controls, all at 60 days of age, which matches well the 8–9 weeks of age in most groups. Control pressures were averaged from the two studies. *Fbln5*$^{-/-}$ animals were significantly older than 60 days, but blood pressure was assumed to be similar at 21 weeks based on the observation of stable geometrical and mechanical properties between 8 and 14 weeks of age by Wan et al.[49] *Fbn1*$^{mgR/mgR}$ pressures were measured by[40] using a different anesthetic, catheterization method, and older mice. Control pressures were used to simulate the mechanics of elastase-treated carotids *in vivo*. All data are presented as mean ± standard error of the mean. An * denotes a significant difference with respect to control based on one-way ANOVA, with a *post-hoc* Bonferroni correction, and a $p < 0.05$ significance level.

	Control	*Eln*$^{+/-}$	*Fbn1*$^{mgR/mgR}$	*Fbln5*$^{-/-}$	Elastase
n	16	6	6	5	7
Age (weeks)	9.0 ± 0.4	8.0 ± 0	8.0 ± 0.2	21.3 ± 0.7*	8.2 ± 0.3
Body Mass (g)	22.9 ± 0.9	25.2 ± 0.8	20.1 ± 2.3	33.0 ± 2.2*	21.7 ± 0.9
Systolic Blood Pressure (mm Hg)					
Systolic	110[a,b]	128[a]	131[c]	112[b]	110[a,b]
Pulse	35[a,b]	48[a]	43[c]	48[b]	35[a,b]
Unloaded Dimensions					
Outer Diameter (μm)	394 ± 8	374 ± 11	399 ± 6	417 ± 13	693 ± 17*
Wall Thickness (μm)	94 ± 4	81 ± 5	94 ± 5	72 ± 4*	27 ± 1
In-vitro Axial Length (mm)	4.66 ± 0.21	5.91 ± 0.20	4.14 ± 0.43	5.42 ± 0.34	7.80 ± 0.5*
Systolic Dimensions					
Outer Diameter (μm)	641 ± 9	592 ± 11	656 ± 16	554 ± 12*	734 ± 20*
Wall Thickness (μm)	26 ± 1	25 ± 2	28 ± 1	34 ± 2*	24 ± 1
In-vivo Axial Stretch	1.72 ± 0.02	1.68 ± 0.03	1.61 ± 0.03*	1.40 ± 0.02*	1.06 ± 0.02*
Systolic Cauchy Stresses (kPa)					
Circumferential	164.5 ± 4.6	190.4 ± 14.3	186.9 ± 5.6	109.2 ± 10.1*	215.1 ± 17.5*
Axial	190.4 ± 7.1	225.3 ± 20.4	164.8 ± 6.2	142.0 ± 16.4	176.0 ± 14.2
Systolic Stiffness (MPa)					
Circumferential	1.30 ± 0.09	1.88 ± 0.23	1.78 ± 0.10	1.07 ± 0.17	6.83 ± 1.32*
Axial	2.75 ± 0.23	4.52 ± 0.46*	2.45 ± 0.29	3.29 ± 0.37	3.97 ± 0.66
Stored Energy (kPa)					
Systole	48.6 ± 2.2	49.4 ± 4.7	36.4 ± 1.5*	22.7 ± 2.2*	7.8 ± 0.6*
Cardiac Cycle	11.5 ± 1.1	12.0 ± 2.0	9.1 ± 0.9	7.6 ± 0.9	3.2 ± 0.8*

Results

Table 1 provides morphometric, hemodynamic, geometric, and mechanical information for all 5 groups: control, $Eln^{+/-}$, $Fbn1^{mgR/mgR}$, $Fbln5^{-/-}$, and elastase-treated. Figure 1 shows mean pressure—diameter behaviors at group-specific values of axial stretch, and axial force-axial stretch responses at a common pressure of 100 mmHg. Note the marked decrease in extensibility with the loss of elastic fiber integrity, as evidenced by decreasing values of mean *in vivo* axial stretch from 1.72 (control) to 1.68 ($Eln^{+/-}$), 1.61 ($Fbn1^{mgR/mgR}$), 1.40 ($Fbln5^{-/-}$), and especially elastase-treated (1.06) vessels. Acute enzymatic removal of elastin also causes a marked dilatation and loss of distensibility, consistent with a vessel consisting primarily of collagen fibers having modest undulation.[20] Control and elastase-treated CCAs thus served as upper and lower bound behaviors for the three genetically modified models. As it can be seen, the pressure—diameter behavior of $Fbn1^{mgR/mgR}$ carotids is most like that of the control while the behavior of the $Eln^{+/-}$ carotids is qualitatively similar, but shifted to the left due to smaller radii. Although similar at low pressures, the behavior of the $Fbln5^{-/-}$ group differs most from that of the control at physiologic pressures. These structural (P—d, f—l) responses are relevant to *in vivo* effects of the wall on the hemodynamics, but material (stress-stretch) behaviors reveal intrinsic properties.

Figure 2 shows the associated mean stress-stretch behaviors in circumferential and axial directions, while Table 2 lists associated values of the best-fit model parameters. Comparing pressure—diameter and circumferential stress-stretch responses reveals the utility of the latter in characterizing material behavior independent of geometry. The stress-stretch responses "fanned-out" and revealed more clearly the different degrees of distensibility, which tend to mirror losses of extensibility. In particular, the $Fbln5^{-/-}$ mutation yielded the most severe elastopathy of the genetically modified models (including the lowest value of *in vivo* axial stretch). Although we are tempted to interpret these results by stating that the $Fbln5^{-/-}$ carotid is the "stiffest", it is better to observe that it is simply the least distensible and extensible of the three mutant models. Indeed, computations under *in vivo* loads reveal that circumferential stiffness is similar amongst controls and genetically modified models, though it is significantly higher in elastase-treated vessels. Axial stiffness is significantly higher in $Eln^{+/-}$ vessels and generally higher in the elastase-treated vessels. To avoid interpretative issues that arise because of pressure dependence, we calculated biaxial stiffness over a fixed range of blood pressures (50—150 mmHg). Figure 3 shows that stiffness increases nearly linearly with associated values of stress, as expected of a highly nonlinear (exponential) material behavior,[34] with circumferential results very similar across all models except elastase-treated. Note that changes due to elastase treatment result from an acute insult, not a germline mutation, the latter of which allow possible compensatory remodeling throughout development. That neither circumferential nor axial material stiffness differed dramatically between the mutants and control, when computed at individual *in vivo* axial deformations, may reflect mechanobiologically favorable compensatory responses of CCAs during development in these mice.

Recalling that the primary function of a large artery is to store elastic energy, Fig. 4 shows iso-energy contours for all 5 groups plus associated histological sections. By plotting energy as a function of biaxial stretch (circumferential along the ordinate and axial along the abscissa), one can easily visualize the degrees of distensibility, extensibility, and anisotropy. Again, control and elastase-treated vessels provide natural upper and lower bounds of elastic fiber integrity. Despite having smaller diameters, $Eln^{+/-}$ carotids exhibit an adaptive increase in medial lamellar units that results in near normal values of energy storage at systole (Table 1). $Fbn1^{mgR/mgR}$ carotids store less energy and exhibit a stronger anisotropy than controls or $Eln^{+/-}$

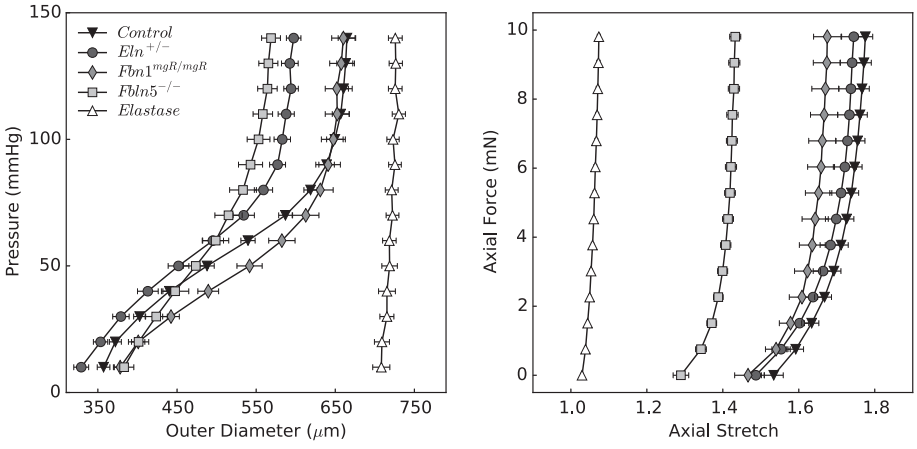

Figure 1 Structural behavior of common carotid arteries upon biaxial testing. Data are presented as mean ± standard error of the mean, with each curve representing the average of the respective experimental group. The left panel shows pressure—diameter responses during inflation tests at the estimated values of *in vivo* axial stretch; the right panel shows axial force-stretch responses at a common distending pressure of 100 mmHg. Note the considerable reproducibility achieved under computer-control.

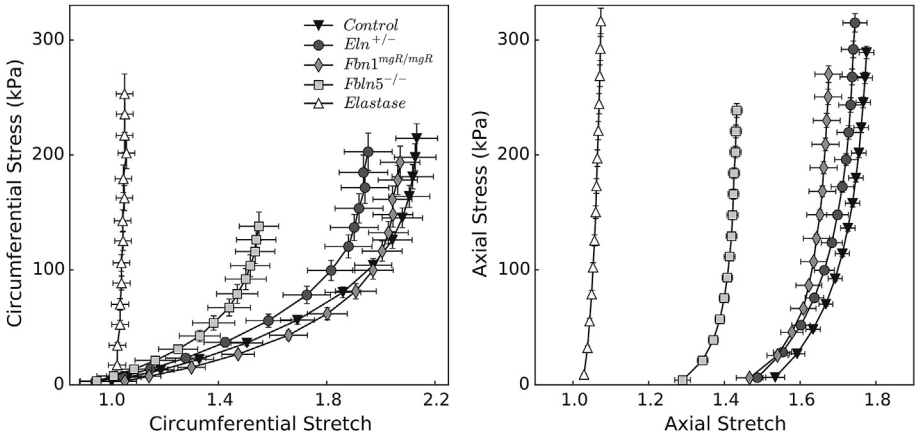

Figure 2 Material properties of common carotid arteries with different degrees of elastic fiber integrity. By treating carotid arteries as thin-walled cylinders, one can calculate principal deformations and stresses from experimental data simply by imposing mechanical equilibrium (see Appendix). Cauchy stress-stretch responses are shown for inflation tests at the estimated values of *in vivo* axial stretch (circumferential properties, left panel), and for extension tests at 100 mmHg (axial properties, right panel). Note the different scales for circumferential and axial stretches. Propagation of experimental errors was calculated using the basic theory of error analysis,[65] taking into account errors in the unloaded configuration and each of the loaded configurations.

Table 2 Best-fit values of model parameters describing the constitutive behavior of common carotid arteries during unloading. Detailed descriptions of the theoretical model and nonlinear regression methods can be found in[23]; see, too, the Appendix for a brief summary.

	Elastic fibers	Axial collagen		Circumferential collagen		Diagonal collagen			RMSE
	c (kPa)	c_1^1(kPa)	c_2^1	c_1^2 (kPa)	c_2^2	$c_1^{3,4}$ (kPa)	$c_2^{3,4}$	α_0 (°)	
Control	8.610	9.299	0.142	4.467	0.045	0.015	1.184	29.011	0.098
$Eln^{+/-}$	11.753	9.645	0.176	5.104	0.088	9.46×10^{-4}	2.156	30.922	0.095
$Fbn1^{mgR/mgR}$	6.928	0.301	1.174	0.937	0.179	1.436	0.554	31.988	0.119
$Fbln5^{-/-}$	21.233	2.171	2.581	4.551	0.833	0.015	6.505	26.282	0.079
Elastase	6.78×10^{-12}	126.976	17.906	5.84×10^{-8}	7.00×10^{-13}	919.416	23.724	46.988	0.282

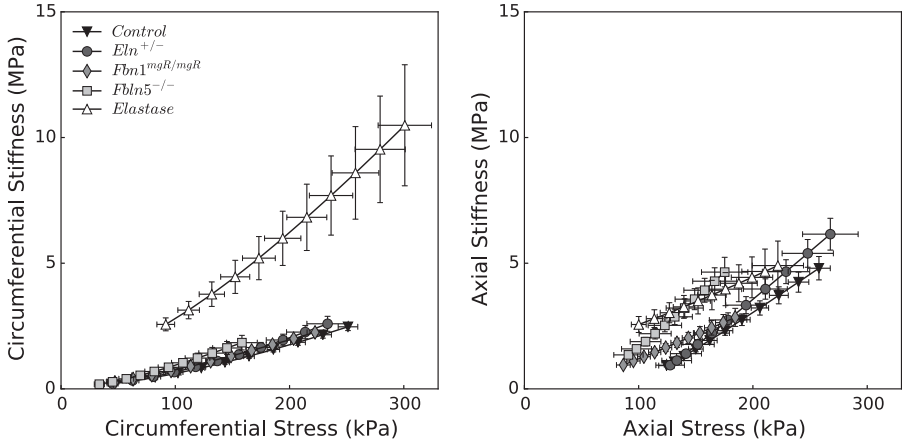

Figure 3 Material stiffness plotted versus Cauchy stress for the five groups of common carotid arteries. All three genetic models lie on the same circumferential stiffness—stress relationship as the control (left panel), while more heterogeneity is observed axially (right panel). Elastase-treated carotids display the most abnormal behavior, with significantly higher circumferential stiffness values at all pressures. This finding suggests that *in vivo* stiffness depends largely on the non-elastin components of the matrix, at least given the pressures considered.

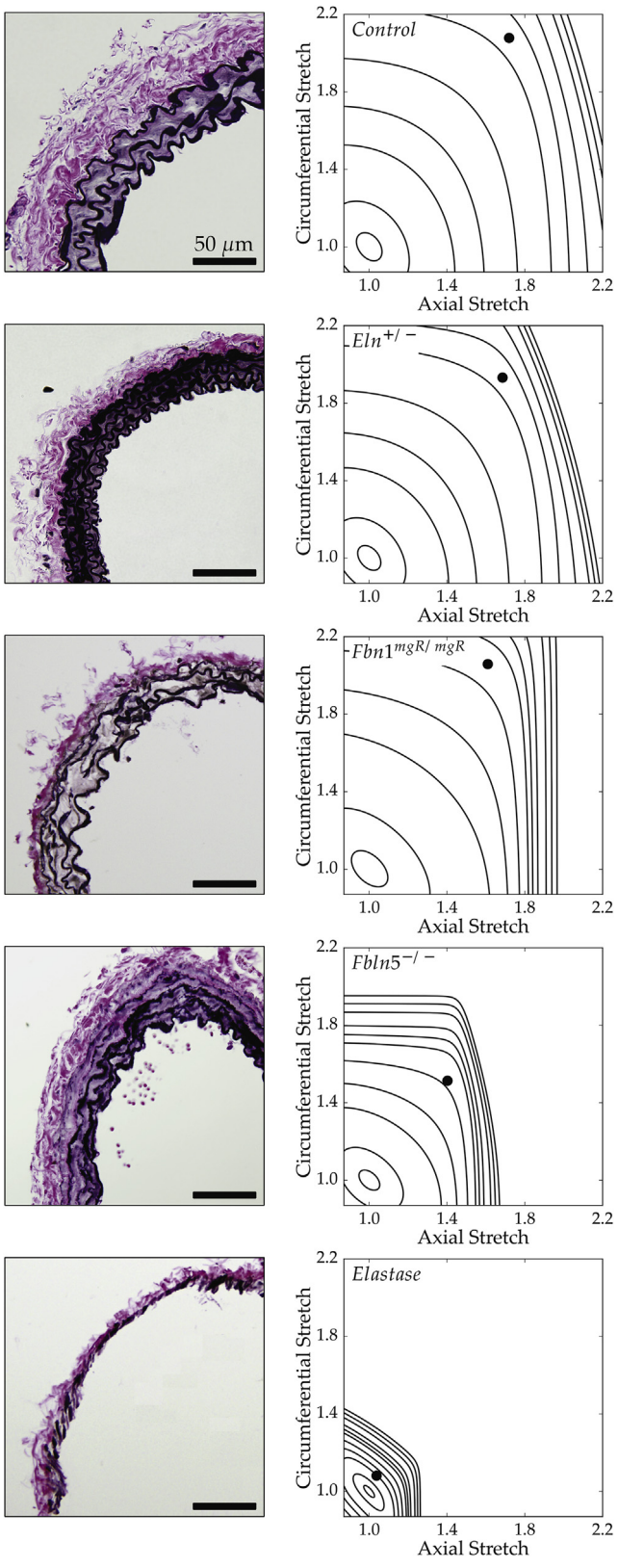

Figure 4 Bright-field microscopy images of Verhoeff Van Gieson (VVG) stained histological cross sections (left column) paired with stored energy contours calculated as a function of biaxial stretches (see Appendix). Filled circles represent *in vivo* energy values computed at group-specific values of *in vivo* axial stretch and systolic pressure relative to an unloaded configuration. This qualitative comparison shows that less energy is stored elastically for greater degrees of elastic fiber insult.

vessels, primarily due to the well-known reduction of *in vivo* axial stretch.[20,29] Their anisotropic energy map is consistent with the hypothesis[26] that an accelerated loss of elastic fibers in Marfan mouse models (confirmed by focal interruptions in the lamellar structure) is compensated by a reduced axial stretch, which helps to promote physiologic levels of distensibility, stress, and stiffness. *Fbln5*$^{-/-}$ carotids exhibit the most dramatic reduction in energy storage, that is, the most severe elastopathy of the three mutants. These vessels are distinguished by a more generalized elastic fiber fragmentation, particularly in the outer media, with clusters of nonfunctional (i.e., non-load bearing) elastin neighboring the main lamellar structures; this radial gradient in elastic matrix disorganization is similar to that previously reported in the thoracic aorta of these mice.[35,36] It appears that the confined stored energy contours and modest values of energy storage at systole result from these underlying structural deficiencies, which prevent *Fbln5*$^{-/-}$ vessels from undergoing normal axial and circumferential deformations. Indeed, results from elastase-treated carotids show that a near total loss of elastin results in minimal axial and circumferential deformations and the lowest degree of elastic energy storage, both of which result in part from a near immediate engagement of adventitial collagen upon loading.

Figure 5 highlights these differences in biaxial deformations and energy storage across groups. Circumferential and especially axial stretches diminish with loss of elastic fiber integrity, with a pattern for the *in vivo* axial stretch that matches closely the loss of energy storage at systolic pressure. When calculated relative to the unloaded state, systolic energy storage in *Fbn1*$^{mgR/mgR}$, *Fbln5*$^{-/-}$, and elastase-treated carotids is, respectively, 74.9%, 46.7%, and 16.0% of normal; when calculated over a single cardiac cycle (see Appendix), cyclic energy storage for the same mutants is 79.1%, 66.1%, and 27.8% of normal. The latter reductions did not reach statistical significance in any of the genetic models, however. Nevertheless, these results highlight how loss of elastic fiber integrity primarily affects arterial extensibility, which in turn is a key determinant of total energy storage.

Energy storage — like stress, material stiffness, and most other mechanical metrics — depends on the value of the distending pressure. Figure 6 shows that stored energy increases gradually with pressure, at group-specific fixed values of axial stretch, with all five models preserving their relative energy storage capability. Although energy storage is a functional-metric of intrinsic material behavior, it cannot be measured directly *in vivo*. More convenient metrics of structural behavior are often measured and compared. Figure 6 also shows values of local pulse wave velocity (*PWV*), estimated using the Moens—Korteweg equation (see Appendix), for all five groups as a function of pressure. With the exception of elastase-treated vessels, values of *PWV* are indistinguishable between control and mutant arteries; they simply vary nearly linearly with the distending pressure.

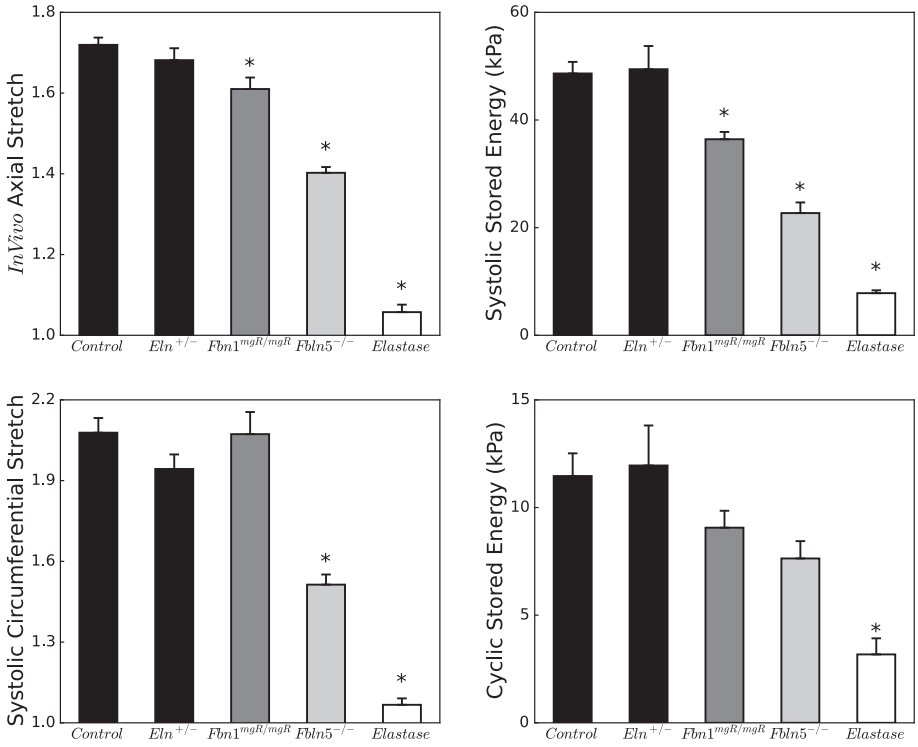

Figure 5 Biaxial stretches (left column) and stored energies (right column) under physiologic conditions. Note the different scales for the stretches, with axial stretches exhibiting a more limited range due to the well-known anisotropy of the arterial wall. Stored energies computed at individual systolic pressures are similar between control and *Eln*$^{+/-}$ carotids, but decrease progressively in *Fbn1*$^{mgR/mgR}$, *Fbln5*$^{-/-}$, and elastase-treated carotids, following a trend similar to the *in vivo* axial stretch. Relative energy storage (over a cardiac cycle) follows the same pattern as total energy storage but loses statistical significance with $n = 5–7$. The * indicates significant differences ($p < 0.05$) with respect to control. Corresponding numerical values can be found in Table 1.

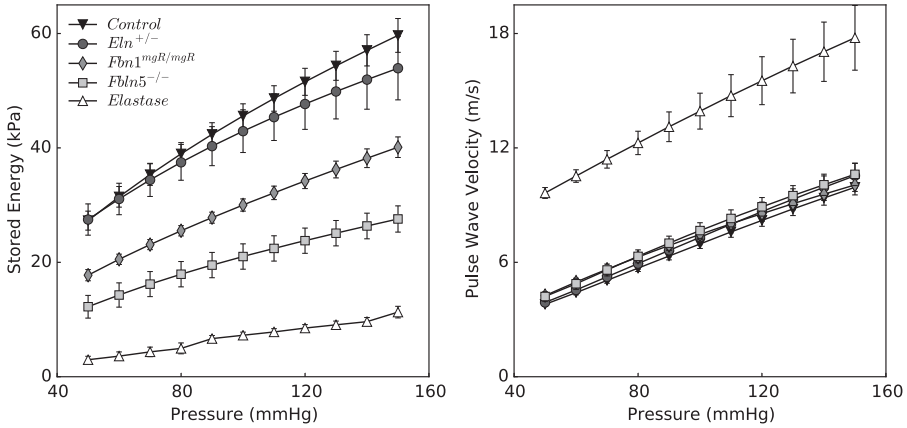

Figure 6 Stored energy (left panel) and computed local pulse wave velocity (right panel) plotted over a wide range of pressures. Trends shown in Table 1 and Fig. 5 for the energy storage at systolic pressures are valid at all pressures, confirming the sensitivity of this metric to distinguish different degrees of elastic fiber functionality. In comparison, pulse wave velocity calculated according to the Moens–Korteweg equation does not show the same descriptive trend.

Discussion

The human common carotid artery becomes progressively less distensible with increasing age,[37] which appears to increase the risk of neurovascular-related conditions, including stroke.[38] Distensibility and similarly pulse wave velocity, which reflect underlying structural stiffness, are convenient to measure and correlate with current or future clinical presentation, but they do not capture well the fundamental function of a central artery - storage and use of elastic energy. To glean increased insight, we measured pressure–diameter and axial force–length behaviors of

murine common carotid arteries *in vitro*, which yielded information sufficient for quantifying stored energy as well as for computing common metrics of structural behavior (pulse wave velocity) and intrinsic material behavior (biaxial stress–strain relations and material stiffness). Despite being beyond the scope of the current study, combining information on biaxial mechanical properties gleaned *in vitro* with non-invasive assessments of distensibility *in vivo* should allow one to estimate the energy stored by the arterial wall under physiologic conditions while accounting for contributions of other factors that remain hard to quantify (e.g., effects of surrounding perivascular tissue on pressure-induced distention). We suggest, therefore, that a mechanistic understanding of the biomechanical factors underlying common prognostic indexes of cardiovascular function can only be achieved by accounting for the evolving multiaxial material properties of the arterial wall, whether during normal aging, hypertension, or progressive disease conditions.

Given the fundamental importance of elastic fibers to central artery structure and function, it is not surprising that many investigators have used mouse models (cf.[33,39]) to assess contributions of these fibers to arterial mechanics (e.g.,[20,29,30,40–49]). In particular, such studies generally report an increased stiffness due to loss of elastic fiber integrity, often inferred from pressure–diameter responses. The stiffness so inferred is necessarily a structural stiffness, which includes effects of both material stiffness and geometry. Our results are consistent with those of many prior studies, but emphasize further the importance of assessing the storage of elastic energy and biaxial material (intrinsic) stiffness. These quantities can best be evaluated from biaxial tests wherein both pressure and axial force are varied.[23] Of the aforementioned studies, only four report complete biaxial data[20,29,30,49] and ours is the first to employ a consistent approach to contrast biaxial behaviors across multiple mouse models to assess graded effects of lost elastic fiber integrity.

The present findings confirm recent results that mean circumferential material stiffness differs little in CCAs from controls and multiple mutant models, including muscular dystrophy, smooth muscle α-actin deficient, and aortic banding models.[27] In contrast, other reports had suggested an increased circumferential modulus in some of these same mutants, which seemed intuitive. For example, there was an early report of a 4-fold increase in Young's modulus in the descending thoracic aorta of the *Fbn1*$^{mgR/mgR}$ mouse[40]; this estimate was based on pulse wave velocity measured *in vivo* and inference of a modulus via the Moens–Korteweg equation. We adopted the opposite approach (see Appendix): we computed material stiffness directly from biaxial data collected *in vitro* and used circumferential values in the Moens–Korteweg relation to calculate pulse wave velocity (*PWV*). Similar to the circumferential stiffness, calculated values of *PWV* did not differ significantly between the genetically modified and control vessels considered here (Fig. 6). Although these calculations allowed a direct comparison of our results with prior *in vivo* findings, we must remember that the Moens–Korteweg equation yields a gross approximation because of its many simplifying assumptions, not the least of which is neglect of axial prestress. Given that axial mechanics can influence strongly the propagation of a pressure wave,[50,51] recall that we found that a decreased axial stretch and stress (Table 1) helps to restore circumferential material stiffness toward normal levels (Fig. 3). It is thus important to account for the overall biaxial state. As noted previously, decreases in axial stretch appear to be early compensatory responses that allow an artery to unload itself both axially and circumferentially in response to diverse genetic or hemodynamic challenges.[26] Although protective and often effective, extreme axial unloading can also render the vessel subject to lateral bending, which can manifest *in vivo* as tortuosity. Interestingly, varying degrees of tortuosity arise in central arteries of *Eln*$^{+/-}$,[42,45] *Fbn1*$^{mgR/mgR}$,[52] and *Fbln5*$^{-/-}$ mice.[36] Consistent with these findings, significant lengthening occurs with acute elastase treatment,[20] which decreases axial stretch dramatically (Table 1). There is a need to study further this important characteristic of compromised elastic fiber integrity.

Among the three mutant models studied herein, deletion of the elastin-associated glycoprotein fibulin-5 resulted in the most severe elastopathy. Fibulin-5 is thought to be involved in elastogenesis.[18] Consequently, associated differences in mechanical behavior manifest early in the central arteries of these mice and, interestingly, progress little thereafter.[49,53] In contrast, fibrillin-1 is thought to contribute to the long-term stability of elastic fibers, literally helping to protect these fibers against the mechanical fatigue that results from cyclic loading.[17] That the biomechanical phenotype of *Fbn1*$^{mgR/mgR}$ CCAs, at 8 weeks of age, was mild may suggest that the appearance of breaks in elastic fibers in single cross-sections (Fig. 4) may not reflect a largely preserved underlying 3-D connectivity of these fibers. There is a need to consider two other key parameters, however: regional location and age. A more severe phenotype would be expected in the ascending aorta, which is subjected to full biaxial loading upon each beat of the heart, and with increasing age due to the accumulative effects of cyclic loading and earlier wave reflections resulting in increased central pulse pressures (*cPP*).[54] Indeed, albeit at a lower rate, mechanical properties deteriorate with age in the aorta of another mouse model of Marfan syndrome (*Fbn1*$^{C1039G/+}$, see[43]), which has an overall less severe aortic phenotype than the *Fbn1*$^{mgR/mgR}$ mouse.

Mechanical properties of central arteries have been studied extensively in the elastin haploinsufficient (*Eln*$^{+/-}$) mouse.[41,42,44,45,47] Consistent with prior reports, we found that, with respect to controls, *Eln*$^{+/-}$ carotids have a decreased arterial size (Fig. 1), increased number of elastic laminae (Fig. 4), and yet similar circumferential properties upon pressurization at their *in vivo* length (Table 1 and Fig. 2). In contrast with prior reports,[42,45,47,55] however, no significant differences were observed in the *in vivo* axial stretch (Table 1 and Fig. 5), which was only slightly reduced with respect to controls. This discrepancy could be due to consistent methodological differences. For example, the *in vivo* axial stretch was previously inferred locally from motions of small affixed charcoal particles upon surgical removal of the vessel,[42] noting that surgical access requires a repositioning of the neck from its native orientation. In contrast, we estimate this stretch (λ_z^{iv}) globally by finding the loaded length *in vitro* at which the artery produces nearly constant axial forces upon pressurization.[31,32]

Differences could thus result from heterogeneities in local axial stretch and their relationship with the global axial stretch or manipulations of the vessel *in situ* (repositioning of the neck) versus *in vitro* (co-axial alignment within the testing device). To confirm our findings, we repeated experiments on mice from a different $Eln^{+/-}$ colony, yet results ($\lambda_z^{iv} = 1.64 \pm 0.04$, $n = 4$) were consistent with our initial findings ($\lambda_z^{iv} = 1.68 \pm 0.03$, $n = 6$). Thus, for elastin haploinsufficient mice available to us, which have ~60% of the normal content of elastin based on histology, compensatory adaptations may have rearranged wall constituents and reduced caliber to maintain mechanical functionality nearly normal, at least for biaxial mechanics and energy storage.

Two of the major consequences of large artery stiffening in humans is an increased *cPP*, which increases the workload on the heart, and an increased propagation of undamped pressure waves to the microcirculation, which is thought to contribute to damage in low resistance end-organs.[8,56,57] Increases in *cPP* have been observed in genetic models of altered elastic fiber integrity, particularly $Eln^{+/-}$ and $Fbln5^{-/-}$ mice (cf. Table 1), yet basic mechanisms underlying a high *cPP* could differ between these two models. There is mounting evidence, for example, that high *cPP* in elastin haploinsufficiency is due to increased systolic pressure.[41,42,45,47,55,58] Although most of these investigations focused on central arteries, a recent study suggested that high blood pressure in $Eln^{+/-}$ mice is caused, in part, by structural and functional alterations of the resistance vasculature,[59] including impaired endothelial function and increasing sensitivity to vasoconstriction in response to angiotensin II. The current findings of nearly normal axial stretches and resilience in $Eln^{+/-}$ CCAs, together with maintenance of circumferential material stiffness, supports the concept that high *cPP* may result primarily from increased peripheral resistances — and associated early wave reflections — in elastin insufficiency. The scenario seems to differ in mice lacking fibulin-5, in which loss of central artery function is also diffuse but more severe.[24] Although high *cPP* was initially thought to be caused by increased systolic pressure,[35] new evidence suggests that systolic pressure is maintained near normal levels while diastolic pressure is decreased ([53] as well as unpublished observations from our laboratory on male mice). In terms of compensatory adaptations, a lower diastolic pressure shifts the response to a more compliant portion of the *P—d* curve, thus minimizing the impact of severe structural alterations on the distensibility of central arteries. By decreasing coronary perfusion pressure, however, a lower central diastolic pressure could yet have negative effects on diastolic function of the heart.[53] These observations highlight the need to distinguish between central and peripheral contributions to high central pulse pressures.

Toward this end, we emphasize that computation of elastic energy storage is very appropriate for evaluating mechanical functionality of large (elastic) arteries because their primary function is to store and then use elastic energy to facilitate flow. In contrast, the primary functions of muscular arteries and arterioles are to regulate blood pressure and flow via vasoconstriction and vasodilatation, that is, changing smooth muscle contractility. Hence, different metrics focusing on active smooth muscle properties would be more appropriate for evaluating their mechanical competence. We did not contrast possible changes in active biaxial properties in the carotids because levels of *in vivo* basal tone are not known and could differ. Clearly, there is a pressing need for more attention to active properties.

In conclusion, our findings suggest that intramural cells may attempt to maintain values of circumferential stress and stiffness (Table 1) near those that are established via normal development while offsetting altered hemodynamic loads by changing structural stiffness. Maintenance of mean circumferential stress is consistent with a seminal observation that the tension per lamellar unit tends to be similar across mammalian species,[60] despite very different arterial dimensions from mice to humans, as well as the provocative observation that circumferential material stiffness tends to be similar across invertebrates and vertebrates.[61] Such maintenance is also consistent with a preferred micromechanical environment for cell sensing and regulation of matrix. There is, therefore, a need for more study of the implications of controlling matrix stiffness on cellular mechanobiological responses.[62] Notwithstanding the important implications of maintaining circumferential stiffness and stress, there is yet a need to consider hemodynamic implications of increasing the structural stiffness and structural implications of axial unloading, which appeared to dictate the graded reduction in energy storage with loss of elastic fiber integrity and was the most striking finding herein (Figs. 4 and 5). Given that energy storage and usage is the most fundamental mechanical function of a large artery, and that damage to or degradation of elastic fibers is one of the hallmarks of arterial aging and hypertension, it is this irreversible biomechanical change that likely most affects cardiac function and flow augmentation. There is a need, therefore, to similarly investigate these characteristics along the aorta, which is responsible for the majority of systemic compliance.

Conflicts of interest statement

The authors declare no conflicts.

Acknowledgment

This work was funded, in part, by a grant from the NIH (R01 HL105297) and grants from the National Marfan Foundation.

Appendix

Data from computer-controlled biaxial mechanical tests were used to calculate mean values of wall stress (σ) and stretch (λ) in both circumferential (ϑ) and axial (z) directions using standard formulae,[63] namely

$$\sigma_\vartheta = \frac{Pa}{h}, \quad \sigma_z = \frac{f + \pi a^2 P}{\pi h(2a + h)}, \quad \lambda_\vartheta = \frac{a + h/2}{A + H/2}, \quad \lambda_z = \frac{\ell}{L},$$

where P, f, a, h,A, H,ℓ, L are the *in vitro* experimentally measured distending pressure, transducer-measured axial force, deformed inner radius, deformed wall thickness,

undeformed inner radius, undeformed wall thickness, deformed axial length, and undeformed axial length, respectively. Stress is, therefore, a convenient measure of "force intensity" having units of force per (oriented) area. The *in vivo* axial stretch — denoted herein as λ_z^{iv} — is defined as the axial stretch at which the artery maintains a nearly constant axial force upon P—d testing between 10 and 140 mmHg. It can be reliably quantified *in vitro* by finding the intersection (or "cross-over point") of the mechanical responses measured from f—l testing at 60, 100, and 140 mmHg[23] and it corresponds well with the ratio of the *in vivo* to the unloaded *in vitro* length of the excised segment.

Whereas pressure—diameter (P—d) and axial force—length (f—l) data reveal the structural behavior of an artery (and depend on geometry), stress-stretch data (from which energy is calculated) reveal the intrinsic material behavior. Constitutive modeling of the arterial behavior was based on the following stored energy function[23]

$$W=\frac{c}{2}(I_C-3)+\sum_{i=1}^{4}\frac{c_1^i}{4c_2^i}\left(\exp\left[c_2^i\left(IV_c^i-1\right)^2\right]-1\right),$$

where $I_C=tr\mathbf{C}=\lambda_r^2+\lambda_\vartheta^2+\lambda_z^2$, $IV_C^i=\mathbf{C}:\mathbf{M}^i\otimes\mathbf{M}^i$ ($\mathbf{C}=\mathbf{F}^T\mathbf{F}$ and $\mathbf{F}=\mathrm{diag}[\lambda_r,\lambda_\vartheta,\lambda_z]$, both measures of the finite deformation, λ_i the principal stretches, and $\lambda_r=1/\lambda_\vartheta\lambda_z$ by incompressibility), and c, c_1^i, c_2^i are material parameters. Note, too, that $\mathbf{M}^i$ denote orientations of four fiber families in the undeformed configuration (axial, circumferential, and two symmetric-diagonal families having the same material parameters but identified by an $\pm$ angle relative to the axial direction). This functional form for the stored energy was motivated by second harmonic generation and two photon fluorescence microscopic examinations of the collagen and elastic fibers.[20] For each of the experimental groups, nonlinear regression was performed to identify the 8 model parameters (Table 2) using standard methods,[23] thus allowing calculation of the stored energy values for any combination of axial and circumferential stretches and subsequent visualization as iso-energy contours (Fig. 4). In addition, based on literature data for systolic and pulse pressures, the circumferential stretches were evaluated at systole and diastole by solving a simple inverse problem,[27] which allowed us to compute the systolic stored energy W^{sys} and the energy stored over a single cardiac cycle $\Delta W=W^{sys}-W^{dia}$ (Table 1 and Fig. 5), where W^{dia} represents the energy existing at diastole.

Due to the nonlinear behavior of the carotid artery wall (Figs. 1 and 2), stiffness depends strongly on the combination of distending pressures and axial stretches imposed experimentally. Values of material stiffness useful in hemodynamic computations can thus be inferred by linearizing the stress-stretch behavior represented by the stored energy function W for any state of mechanical loading desired.[64] Linearized elastic moduli were calculated as

$$\mathbb{C}_{ijkl}=2\delta_{ik}F^o_{lA}F^o_{jB}\frac{\partial W}{\partial C_{AB}}\bigg|_{C^o}+2\delta_{jk}F^o_{iA}F^o_{lB}\frac{\partial W}{\partial C_{AB}}\bigg|_{C^o}$$
$$+4F^o_{iA}F^o_{jB}F^o_{kP}F^o_{lQ}\frac{\partial^2 W}{\partial C_{AB}\partial C_{PQ}}\bigg|_{C^o},$$

where ∂ indicates the partial derivative operator while the superscript "o" denotes a finite deformation corresponding to physiologic loads and $\delta_{ij}=1$ if $i=j$ or 0 if $i\neq j$, for any $i,j=1,2,3$. We used values of systolic blood pressure to evaluate the second-order tensors $\boldsymbol{F}^o$ and $\boldsymbol{C}^o$ and then calculate associated values of material stiffness in both axial ($\mathbb{C}_{zzzz}$) and circumferential ($\mathbb{C}_{\vartheta\vartheta\vartheta\vartheta}$) directions (Table 1). Pulse wave velocity — an index of structural stiffness — was calculated using the Moens—Korteweg equation which, for a given distending pressure, combines the circumferential stiffness and the associated geometrical dimensions as $PWV=\sqrt{\mathbb{C}_{\vartheta\vartheta\vartheta\vartheta}h/2\rho a}$ (the density of the artery wall was assumed to be similar to the density of water, that is $\rho=1000\ kg/m^3$). The Moens—Korteweg equation only provides an estimate, of course, given the many simplifying assumptions underlying its derivation.

Studies of the sensitivity of values of stored energy, material stiffness, and pulse wave velocity (*PWV*) to the value of pressure used in the calculation are shown in Figs. 3 and 6 by repeating the calculations for different values of distending pressure from 50 to 150 mmHg. All calculations in this work were based on the assumption that the axial stretch remains constant during the cardiac cycle and equal to the *in vivo* axial stretch λ_z^{iv}. Finally, note that we computed *PWV* since it depends only on the measurable geometry and material properties. We did not calculate the often reported metric of distensibility (which reflects changes in diameter due to changes in pressure from diastole to systole) since *in vivo* values depend on the tethering effect of perivascular tissues, which was not known for the five different mouse models.

References

1. Clark JM, Glagov S. Transmural organization of the arterial media. The lamellar unit revisited. *Arterioscler Thromb Vasc Biol* 1985;**5**(1):19—34.
2. Wagenseil JE, Mecham RP. Vascular extracellular matrix and arterial mechanics. *Physiol Rev* 2009;**89**(3):957—89.
3. Davis EC. Stability of Elastin in the developing mouse Aorta: a quantitative radioautographic study. *Histochemistry* 1993;**100**(1):17—26.
4. Davis EC. Elastic lamina growth in the developing mouse aorta. *J Histochem Cytochem* 1995;**43**(11):1115—23.
5. Arribas SM, Hinek A, González MC. Elastic fibres and vascular structure in hypertension. *Pharmacol Ther* 2006;**111**(3):771—91.
6. Sherratt MJ. Tissue elasticity and the ageing elastic fibre. *AGE* 2009;**31**(4):305—25.
7. Lillie MA, Gosline JM. Limits to the durability of arterial elastic tissue. *Biomaterials* 2007;**28**(11):2021—31.
8. O'Rourke MF, Hashimoto J. Mechanical factors in arterial aging: a clinical perspective. *J Am Coll Cardiol* 2007;**50**(1):1—13.
9. Hornebeck W, Emonard H. The cell-elastin-elastase(s) interacting triade directs elastolysis. *Front Biosci Landmark Ed* 2011;**16**:707—22.
10. Lakatta EG, Wang M, Najjar SS. Arterial aging and subclinical arterial disease are fundamentally intertwined at macroscopic and molecular levels. *Med Clin North Am* 2009;**93**(3):583—604.
11. Lacolley P, Challande P, Osborne-Pellegrin M, Regnault V. Genetics and pathophysiology of arterial stiffness. *Cardiovasc Res* 2009;**81**(4):637—48.
12. Safar ME. Arterial aging — hemodynamic changes and therapeutic options. *Nat Rev Cardiol* 2010;**7**(8):442—9.
13. Pratt B, Curci J. Arterial elastic fiber structure. Function and potential roles in acute aortic dissection. *J Cardiovasc Surg (Torino)* 2010;**51**(5):647—56.

14. Wilson JS, Baek S, Humphrey JD. Importance of initial aortic properties on the evolving regional anisotropy, stiffness and wall thickness of human abdominal aortic aneurysms. *J R Soc Interface* 2012;**9**(74):2047—58.
15. Maurice P, Blaise S, Gayral S, Debelle L, Laffargue M, Hornebeck W, et al. Elastin fragmentation and atherosclerosis progression: the elastokine concept. *Trends cardiovasc Med* 2013;**23**(6):211—21.
16. Kielty CM. Elastic fibres in health and disease. *Expert Rev Mol Med* 2006;**8**(19):1—23.
17. Ramirez F, Dietz HC. Fibrillin-rich microfibrils: structural determinants of morphogenetic and homeostatic events. *J Cell Physiol* 2007;**213**(2):326—30.
18. Yanagisawa H, Davis EC. Unraveling the mechanism of elastic fiber assembly: the roles of short fibulins. *Int J Biochem Cell Biol* 2010;**42**(7):1084—93.
19. Faury G. Function—structure relationship of elastic arteries in evolution: from microfibrils to elastin and elastic fibres. *Pathol Biol* 2001;**49**(4):310—25.
20. Ferruzzi J, Collins MJ, Yeh AT, Humphrey JD. Mechanical assessment of elastin integrity in fibrillin-1-deficient carotid arteries: implications for Marfan syndrome. *Cardiovasc Res* 2011;**92**(2):287—95.
21. Karnik SK, Brooke BS, Bayes-Genis A, Sorensen L, Wythe JD, Schwartz RS, et al. A critical role for elastin signaling in vascular morphogenesis and disease. *Development* 2003;**130**(2):411—23.
22. Michel J-B. Anoïkis in the cardiovascular system known and unknown extracellular mediators. *Arterioscler Thromb Vasc Biol* 2003;**23**(12):2146—54.
23. Ferruzzi J, Bersi MR, Humphrey JD. Biomechanical phenotyping of central arteries in health and disease: advantages of and methods for murine models. *Ann Biomed Eng* 2013;**41**(7):1311—30.
24. Ferruzzi J, Bersi MR, Uman S, Yanagisawa H, Humphrey JD. Decreased elastic energy storage, not increased material stiffness, characterizes central artery dysfunction in fibulin-5 deficiency independent of sex. *J Biomech Eng* 2015;**137**(3):031007.
25. Gleason RL, Wilson E, Humphrey JD, Gray SP. A multiaxial computer-controlled organ culture and biomechanical device for mouse carotid arteries. *J Biomech Eng* 2005;**126**(6):787—95.
26. Humphrey JD, Eberth JF, Dye WW, Gleason RL. Fundamental role of axial stress in compensatory adaptations by arteries. *J Biomech* 2009;**42**(1):1—8.
27. Bersi MR, Ferruzzi J, Eberth JF, Gleason Jr RL, Humphrey JD. Consistent biomechanical phenotyping of common carotid arteries from seven genetic, pharmacological, and surgical mouse models. *Ann Biomed Eng* 2014;**42**(6):1207—23.
28. Gleason RL, Dye WW, Wilson E, Humphrey JD. Quantification of the mechanical behavior of carotid arteries from wild-type, dystrophin-deficient, and sarcoglycan-δ knockout mice. *J Biomech* 2008;**41**(15):3213—8.
29. Eberth JF, Taucer AI, Wilson E, Humphrey JD. Mechanics of carotid arteries in a mouse model of Marfan syndrome. *Ann Biomed Eng* 2009;**37**(6):1093—104.
30. Wan W, Yanagisawa H, Gleason Jr RL. Biomechanical and microstructural properties of common carotid arteries from fibulin-5 null mice. *Ann Biomed Eng* 2010;**38**(12):3605—17.
31. Van Loon P. Length-force and volume-pressure relationships of arteries. *Biorheology* 1977;**14**(4):181—201.
32. Weizsäcker HW, Lambert H, Pascale K. Analysis of the passive mechanical properties of rat carotid arteries. *J Biomech* 1983;**16**(9):703—15.
33. Wagenseil JE, Mecham RP. Elastin in large artery stiffness and hypertension, J. *Cardiovasc Transl Res* 2012;**5**(3):264—73.
34. Fung YC. Elasticity of soft tissues in simple elongation. *Am J Physiol — Leg Content* 1967;**213**(6):1532—44.
35. Yanagisawa H, Davis EC, Starcher BC, Ouchi T, Yanagisawa M, Richardson JA, et al. Fibulin-5 is an elastin-binding protein essential for elastic fibre development in vivo. *Nature* 2002;**415**(6868):168—71.
36. Nakamura T, Lozano PR, Ikeda Y, Iwanaga Y, Hinek A, Minamisawa S, et al. Fibulin-5/DANCE is essential for elastogenesis in vivo. *Nature* 2002;**415**(6868):171—5.
37. Benetos A, Laurent S, Hoeks AP, Boutouyrie PH, Safar ME. Arterial alterations with aging and high blood pressure. A noninvasive study of carotid and femoral arteries. *Arterioscler Thromb Vasc Biol* 1993;**13**(1):90—7.
38. Laurent S, Katsahian S, Fassot C, Tropeano A-I, Gautier I, Laloux B, et al. Aortic stiffness is an independent predictor of fatal stroke in essential hypertension. *Stroke* 2003;**34**(5):1203—6.
39. Dietz HC, Mecham RP. Mouse models of genetic diseases resulting from mutations in elastic fiber proteins. *Matrix Biol* 2000;**19**(6):481—8.
40. Marque V, Kieffer P, Gayraud B, Lartaud-Idjouadiene I, Ramirez F, Atkinson J. Aortic wall mechanics and composition in a transgenic mouse model of marfan syndrome. *Arterioscler Thromb Vasc Biol* 2001;**21**(7):1184—9.
41. Faury G, Pezet M, Knutsen RH, Boyle WA, Heximer SP, McLean SE, et al. Developmental adaptation of the mouse cardiovascular system to elastin haploinsufficiency. *J Clin Invest* 2003;**112**(9):1419—28.
42. Wagenseil JE, Nerurkar NL, Knutsen RH, Okamoto RJ, Li DY, Mecham RP. Effects of elastin haploinsufficiency on the mechanical behavior of mouse arteries. *Am J Physiol — Heart Circ Physiol* 2005;**289**(3):H1209—17.
43. Chung AWY, Yeung KA, Sandor GGS, Judge DP, Dietz HC, Breemen C van. Loss of elastic fiber integrity and reduction of vascular smooth muscle contraction resulting from the upregulated activities of matrix metalloproteinase-2 and -9 in the thoracic aortic aneurysm in Marfan syndrome. *Circ Res* 2007;**101**(5):512—22.
44. Pezet M, Jacob M-P, Escoubet B, Gheduzzi D, Tillet E, Perret P, et al. Elastin haploinsufficiency induces alternative aging processes in the aorta. *Rejuvenation Res* 2008;**11**(1):97—112.
45. Carta L, Wagenseil JE, Knutsen RH, Mariko B, Faury G, Davis EC, et al. Discrete contributions of elastic fiber components to arterial development and mechanical compliance. *Arterioscler Thromb Vasc Biol* 2009;**29**(12):2083—9.
46. Haskett D, Doyle JJ, Gard C, Chen H, Ball C, Estabrook MA, et al. Altered tissue behavior of a non-aneurysmal descending thoracic aorta in the mouse model of Marfan syndrome. *Cell Tissue Res* 2011;**347**(1):267—77.
47. Le VP, Knutsen RH, Mecham RP, Wagenseil JE. Decreased aortic diameter and compliance precedes blood pressure increases in postnatal development of elastin-insufficient mice. *Am J Physiol — Heart Circ Physiol* 2011;**301**(1):H221—9.
48. Mariko B, Pezet M, Escoubet B, Bouillot S, Andrieu J-P, Starcher B, et al. Fibrillin-1 genetic deficiency leads to pathological ageing of arteries in mice. *J Pathol* 2011;**224**(1):33—44.
49. Wan W, Gleason RL. Dysfunction in elastic fiber formation in fibulin-5 null mice abrogates the evolution in mechanical response of carotid arteries during maturation. *Am J Physiol — Heart Circ Physiol* 2013;**304**(5):H674—86.
50. Atabek HB. Wave propagation through a viscous fluid contained in a tethered, initially stressed, orthotropic elastic tube. *Biophys J* 1968;**8**(5):626—49.
51. Demiray H. Wave propagation through a viscous fluid contained in a prestressed thin elastic tube. *Int J Eng Sci* 1992;**30**(11):1607—20.

52. Schwill S, Seppelt P, Grünhagen J, Ott C-E, Jugold M, Ruhparwar A, et al. The fibrillin-1 hypomorphic mgR/mgR murine model of Marfan syndrome shows severe elastolysis in all segments of the aorta. *J Vasc Surg* 2013;**57**(6). 1628—1636.e3.
53. Le VP, Stoka KV, Yanagisawa H, Wagenseil JE. Fibulin-5 null mice with decreased arterial compliance maintain normal systolic left ventricular function, but not diastolic function during maturation. *Physiol Rep* 2014;**2**(3):e00257.
54. Avolio A. Ageing and wave reflection. *J Hypertens* 1992;**10**(6): S83—6.
55. Wagenseil JE, Knutsen RH, Li DY, Mecham RP. Elastin-Insufficient mice show normal cardiovascular remodeling in 2K1C hypertension despite higher baseline pressure and unique cardiovascular architecture. *Am J Physiol — Heart Circ Physiol* 2007;**293**(1):H574—82.
56. Adji A, O'Rourke MF, Namasivayam M. Arterial stiffness, its assessment, prognostic value, and implications for treatment. *Am J Hypertens* 2011;**24**(1):5—17.
57. Barodka VM, Joshi BL, Berkowitz DE, Hogue CW, Nyhan D. Implications of vascular aging. *Anesth Analg* 2011;**112**(5): 1048—60.
58. Kozel BA, Knutsen RH, Ye L, Ciliberto CH, Broekelmann TJ, Mecham RP. Genetic modifiers of cardiovascular phenotype caused by elastin haploinsufficiency act by extrinsic noncomplementation. *J Biol Chem* 2011;**286**(52):44926—36.
59. Osei-Owusu P, Knutsen RH, Kozel BA, Dietrich HH, Blumer KJ, Mecham RP. Altered reactivity of resistance vasculature contributes to hypertension in elastin insufficiency. *Am J Physiol — Heart Circ Physiol* 2014;**306**(5):H654—66.
60. Wolinsky H, Glagov S. A lamellar unit of aortic medial structure and function in mammals. *Circ Res* 1967;**20**(1):99—111.
61. Shadwick RE. Mechanical design in arteries. *J Exp Biol* 1999; **202**(23):3305—13.
62. Humphrey JD, Dufresne ER, Schwartz MA. Mechanotransduction and extracellular matrix homeostasis. *Nat Rev Mol Cell Biol* 2014;**15**(12):802—12.
63. Humphrey JD. *Cardiovascular solid mechanics: cells, tissues, and organs*. New York: Springer; 2002.
64. Baek S, Gleason RL, Rajagopal KR, Humphrey JD. Theory of small on large: potential utility in computations of fluid—solid interactions in arteries. *Comput Methods Appl Mech Eng* 2007; **196**(31—32):3070—8.
65. Taylor JR. *An introduction to error analysis: the study of uncertainties in physical measurements*. Sausalito, Calif: University Science Books; 1997.